Environmental Science Processes & Impacts

The Precipitation, Growth and Stability of Mercury Sulfide Nanoparticles Formed in Presence of Marine Dissolved Organic Matter.

Journal:	*Environmental Science: Processes & Impacts*
Manuscript ID	EM-ART-12-2017-000593.R1
Article Type:	Paper
Date Submitted by the Author:	16-Feb-2018

Complete List of Authors:	Mazrui, Nashaat; University of Connecticut, Marine Sciences Seelen, Emily; University of Connecticut, Marine Sciences Kingondu, Cecil; South Eastern Kenya University; Botswana International University of Science and Technology Thota, Sravan; University of Connecticut, Chemistry Department Awino, Joseph; University of Connecticut, Chemistry Rouge, Jessica; University of Connecticut, Department of Chemistry Zhao, Jing; University of Connecticut, Chemistry Mason, Robert; University of Connecticut,

Environmental Significance Statement

The precipitation of β-HgS*(s)* nanoparticles in natural systems has been shown to affect the methylation potential of an environment. Here we use marine DOM to precipitate β-HgS*(s)* nanoparticles and investigate how they form and persist under different conditions. Our results describe environmental processes that would impact the formation, stability and toxicity of these nanoparticles in aquatic systems.

The Precipitation, Growth and Stability of Mercury Sulfide Nanoparticles Formed in Presence of Marine Dissolved Organic Matter.

Nashaat M. Mazrui[1,2*], Emily Seelen[2], Cecil K. King'ondu[3,4], Sravan Thota[1], Joseph Awino[1], Jessica Rouge[1], Jing Zhao[1], Robert P. Mason[1,2*]

[1] Department of Chemistry, University of Connecticut, Storrs, CT, USA
[2] Department of Marine Sciences, University of Connecticut, Groton, CT, USA
[3] Department of Chemistry, South Eastern Kenya University, Kitui, Kenya
[4] Department of Chemistry and Forensic Sciences, Botswana International University of Science and Technology, Palapye, Botswana.

***Email:** mzrnash@gmail.com, robert.mason@uconn.edu

Abstract

The methylation of mercury is known to depend on the chemical forms of mercury (Hg) present in the environment and the methylating bacterial activity. In sulfidic sediments, under conditions of supersaturation with respect to metacinnabar, recent research has shown that mercury precipitates as β-HgS*(s)* nanoparticles (β-HgS$(s)_{nano}$). Few studies have looked at the precipitation of β-HgS$(s)_{nano}$ in presence of marine dissolved organic matter (DOM). In this work, we used dynamic light scattering (DLS) coupled with UV-Vis spectroscopy and transmission electron microscopy (TEM) to investigate the formation and fate of β-HgS$(s)_{nano}$ formed in association with marine DOM extracted from the east and west of Long Island Sound, and at the shelf break of the North Atlantic Ocean, as well as with low molecular weight thiols. We found that while β-HgS$(s)_{nano}$ formed in the presence of oceanic DOM doubled in size after 5 weeks, those forming in solutions with coastal DOM did not grow over time. In addition, when the Hg^{II}:DOM ratio was varied, β-HgS$(s)_{nano}$ only rapidly aggregated at high ratios (> 41 μmol Hg^{II} /mg C) where the concentration of thiol groups was determined to be substantially low relative to Hg^{II}. This suggests that functional groups other than thiols could be involved in the stabilization of β-HgS$(s)_{nano}$. Furthermore, we showed that β-HgS$(s)_{nano}$ forming under anoxic conditions remained stable and therefore could persist in the environment sufficiently to impact the methylation potential. Exposure of β-HgS$(s)_{nano}$ to sunlit and oxic environments, however, caused rapid aggregation and sedimentation of the nanoparticles, suggesting that photo-induced changes or oxidation of organic matter adsorbed on the surface of β-HgS$(s)_{nano}$ affected their stability in surface waters.

Introduction

The production of methylmercury (MeHg) from inorganic mercury (Hg^{II}) within environmental systems and its overall toxicity to humans and wildlife has spurred concern over anthropogenic Hg emissions worldwide and prompted research into the processes of MeHg formation. Hg^{II} is converted to MeHg (a more toxic and bio-accumulative form commonly found in the environment) during the remineralization of organic matter by anaerobic bacteria carrying the methylating gene pair hgcA and hgcB.[1, 2] A major hotspot for MeHg production is the coastal sediment, owing to the active degradation of organic matter by sulfate reducing bacteria — one of the main methylators of Hg^{II}.[1, 3-5] Substantial progress in understanding the biogeochemistry of Hg^{II} in coastal areas has been made thus far; however, it is still difficult to predict the relative production of MeHg across ecosystems. While it is known that both the activity of the methylating bacteria and the bioavailability of Hg^{II} influence the extent of net methylation, the speciation of Hg^{II} in sediment porewater is not well understood.[6-11] Mercury forms complexes with different ligands in solution including chlorides, hydroxides, thiols, and inorganic sulfides. As Hg^{II} is a soft acid, its complexes with reduced sulfur groups are the most thermodynamically stable. Recent studies have shown that Hg^{II} can also exist in solution as mercury sulfide nanoparticles (β-$HgS(s)_{nano}$) and these have an enhanced availability to methylating bacteria relative to micro particles of β-$HgS(s)$.[12, 13] While our understanding of the importance of nanoparticles (NPs) to environmental Hg^{II} speciation is gaining ground, little data exists on the formation and persistence of these particles under different conditions. The objective of this work was to gain further knowledge on the formation and behavior of β-$HgS(s)_{nano}$ forming in the environment.

Nanoparticles in the environment have been detected in flood plains, hydrothermal vents, ocean waters, porewaters, and mine tailings.[14-20] Due to their high surface to volume ratio, nanometer sized particles have high surface energy which the particle tends to compensate for by rearranging surface and near surface atoms.[21] As such, NPs (especially those < 30 nm) have size-dependent properties affecting their reactivity, mobility, solubility and bioavailability, and which differ substantially from their bulk counterparts.[12, 13, 21] Due to their high surface energy, NPs are unstable and tend to aggregate, coalesce when possible and settle out of solution.[22, 23]

Organic molecules have been shown to hinder the aggregation of particles by forming coordinate covalent bonds between functional groups on the organic molecule and atoms on the surface of the particle.[24, 25] Nonspecific hydrophobic interactions between humic fractions of natural dissolved organic matter (DOM) and β-HgS*(s)*$_{nano}$ have also been noted to slow down the growth of particles.[26] The adsorption of negatively charged organic matter to the β-HgS*(s)*$_{nano}$ surface enhances electrostatic repulsive forces and induces electrosteric forces hindering the aggregation of β-HgS*(s)*$_{nano}$.[26-31] The β-HgS*(s)*$_{nano}$ formed in the presence of DOM isolated from a terrestrial environment (Suwannee River Humic Acid (SRHA)), were observed under Transmission Electron Microscopy (TEM) to have a diameter of less than 10 nm.[32] Such particles are considered metacinnabar-like as they have an average bond length and coordination number similar to β-HgS*(s)*, but are less crystalline and possess a higher degree of disorder.[29, 31, 32]

Most studies on β-HgS*(s)*$_{nano}$ have focused on fresh water and soil-derived DOM, and little has been done with marine DOM. In addition, few studies have looked at the persistence of the β-HgS*(s)*$_{nano}$ under different environmental conditions. β-HgS*(s)*$_{nano}$ are expected to form in the sediment where it is anoxic and dark; however, their fate and behavior when these conditions

change, remains unknown. For example, previous studies have shown that during sediment resuspension events, trace metals released to ocean waters become oxidized and change their form and speciation.[33] Though the oxidation of HgS*(s)* by itself is known to be a slow process, photo-induced changes to the β-HgS*(s)*$_{nano}$ or to the DOM layer stabilizing the β-HgS*(s)*$_{nano}$ against aggregation could impact NP fate and transport. Here we investigated the size and stability of β-HgS*(s)*$_{nano}$ forming in the presence of various thiols and organic matter extracted from three marine environments: Eastern Long Island Sound (ELIS), Western Long Island Sound (WLIS), and offshore at the shelf break of the North Atlantic Ocean (SB) (Fig. S1). The thiols used in this study include cysteine, glutathione, 4- mercaptophenyl acetic acid (4- MAA), 1,2-ethanedithiol, and 1,3-propanedithiol. Cysteine and glutathione are among the low molecular weight thiols commonly found at nM concentrations in natural waters.[34, 35] These two thiols have also been used in previous studies to precipitate NPs under natural conditions and thus they allow for comparison with earlier studies.[27, 28] 1,2-ethanedithiol, and 1,3-propanedithiol were chosen to evaluate the effect of multiple thiol groups (as found in some proteins) on β-HgS*(s)*$_{nano}$ precipitation. 4-Mercaptophenyl acetic acid is an aromatic thiol and was used to evaluate the effect of an aromatic ring on β-HgS*(s)*$_{nano}$ precipitation. While the main focus of our study was the use of marine DOM to precipitate β-HgS*(s)*$_{nano}$, model thiol ligands were also used to evaluate how the quality of DOM is likely to affect β-HgS*(s)*$_{nano}$ precipitation. Based on results from earlier studies, we hypothesized that: (1) Because of a higher humic fraction, coastal DOM would be better at inhibiting the aggregation of β-HgS*(s)* nanoparticles than DOM from the open ocean; (2) Since DOM prevents the aggregation of β-HgS*(s)* nanoparticles by increasing repulsive forces between particles, increasing the concentration of marine DOM relative to Hg^{II} decreases the extent of the aggregation of β-HgS*(s)* nanoparticles; and (3) Due to the photo-

degradation of marine DOM, the stability of β-HgS*(s)* nanoparticles is reduced under light and in oxic environments.

Methodology

Extracting Dissolved Organic Matter from Seawater

Dissolved organic matter was isolated from surface waters collected at Eastern Long Island Sound (ELIS), Western Long Island Sound (WLIS), and at the shelf break of the North Atlantic Ocean (SB) as shown in the map (Fig. S1). Surface water from each of the locations was collected using Teflon-coated acid cleaned Go-Flo bottles deployed down to the chlorophyll maximum zone. The water was filtered on board immediately after collection using a 0.45 μm and subsequently 0.2 μm cartridge filter and then stored in ultra-clean cubitainers. Marine DOM was extracted from the filtered seawater using a modified benzene styrene polymer cartridge pre-rinsed with 6 mL of methanol and 1 L of ultrapure UV treated water. Filtered seawater (acidified to pH 2) was passed through the rinsed cartridge at a rate of < 4 mL/min using a peristaltic pump.[36] After desalting with 40 mL of 0.01 M HCl and drying the cartridge with Ar/N_2, DOM was eluted using methanol and acetone and then stored in the freezer until use.[36] An aliquot of the DOM in organic solvent was dried using a Nitrogen evaporator (N-EVAP 111) at 40°C, then re-dissolved in purified water or 2.2 mM $NaHCO_3$ (pH 7.8) to be analyzed for the dissolved organic carbon (DOC) concentration or used in experimental solutions, respectively. All DOM solutions were filtered through a 0.2μm filter before use. The absorbance and fluorescence measurements of the extracted DOM were performed as described further below. Also, reduced sulfur groups were quantified using Sulfur X-ray Absorption Near Edge Structure (XANES) as

described in the supporting information for a DOM sample collected in Long Island Sound waters south of Nantucket.

Preparation of Experimental Solutions

All solutions were prepared using UV oxidized deionized water (18.4 MΩ), degassed by boiling and purging with nitrogen for at least 20 min. Preparation and synthesis was done in a nitrogen filled glove box. The mercury stock solution was prepared by dissolving 0.26 g of mercury nitrate monohydrate in 25 mL of 0.1 M HCl. Crystals of sodium sulfide nanohydrate (Acros) were washed to remove oxidation products and dried under nitrogen, and then 10 g of the washed crystals were dissolved in 5 mL of degassed water. The concentration of the sulfide standard was determined by titrating an aliquot of the sulfide preserved in Sulfide Anti-Oxidant Buffer (SAOB) with $Pb(NO_3)_2$ using an ion selective electrode.[37]

Low molecular weight (LMW) thiol capping agents consisting of 1,2-ethanedithiol, 1,3-propanedithiol, 4- mercaptophenyl acetic acid, glutathione, and L-cysteine were obtained from Alfa Aeser. Stock solutions of the dithiols and 4- mercaptophenyl acetic acid (4-MAA) were prepared by dissolving 5 μL and 0.02 g, respectively, in 5 mL methanol. Glutathione and L-cysteine solutions were prepared by dissolving 0.01 and 0.02 g respectively, in 10 mL of 2.2 mM $NaHCO_3$ (pH 7.8). The thiol stock solutions were stored in the glove box and used within 24 h. Aliquots of all prepared solutions were diluted using the reaction matrix (2.2 mM $NaHCO_3$, pH 7.8) before amending them into respective reaction vials. As the pH of the experimental solution was 7.8 and the pK_{a1} of H_2S is 7, dissolved sulfide existed predominantly as HS^-, thus here we use HS^- to refer to the dissolved sulfide in our experimental solutions.

Synthesis of β-HgS*(s)*$_{nano}$

The synthesis of β-HgS*(s)*$_{nano}$ generally followed published procedures used to precipitate naturally forming NPs in the lab.[23, 27] Here, β-HgS*(s)*$_{nano}$ were synthesized by adding an aliquot of the appropriate capping agent (concentration and type given with the results) to the solution matrix followed by Hg^{II} addition. The solution of Hg^{II} and capping agent was mixed end to end, and then HS^- was added and the solution mixed again. The binding of Hg^{II} to DOM has been shown to increase with equilibration time of Hg^{II} with DOM for up to 24 hours.[38] Mercury is known to bind preferentially to S containing sites on DOM, however, these sites are found at a much lower concentration than the weaker O and N containing functional groups.[39, 40] As equilibration time increases therefore, it is assumed that Hg^{II}, which would initially bind to the more abundant oxygen and nitrogen containing functional groups would migrate after an equilibration time of between 10–24 h to the stronger thiol binding sites.[38] To test if the equilibration time of Hg^{II} with DOM, prior to sulfide addition, affected particle size; a subset of the experimental vials were equilibrated with DOM for 24 h before HS^- was added. Particle size with and without Hg^{II}-DOM equilibration was similar (Fig. S2), subsequently, HS^- was added to all vials no more than 5 min after Hg^{II} addition to DOM. For the thiols that were initially dissolved in methanol (i.e the dithiols and 4-MAA), control experiments of glutathione and cysteine were prepared with an equivalent amount of methanol added prior to Hg^{II} and HS^- addition. Cysteine and glutathione vials carried out with and without methanol formed particles of similar size (Fig. S3). Hence it was concluded that the methanol added to aid in the dissolution of the dithiols and 4-MAA did not have an apparent effect on particle formation. Unless otherwise stated, the final concentration of the capping agent was 300 μM for the monothiols,

150 μM for the dithiols, and 833 μM C for DOM. The concentrations of Hg^{II} and HS^- were 150 μM each.

The objective of this study was to investigate the effect of marine DOM on the growth and aggregation of β-HgS*(s)*$_{nano}$ by determining the size of the particles forming under various conditions. All experiments were done in a low ionic strength solution (2.2 Mm $NaHCO_3$), since a high ionic strength would compress the electric double layer reducing repulsive forces between particles and promoting aggregation.[41] As we wanted to study the effect of marine DOM on the aggregation of particles without introducing additional factors bound to affect aggregation; higher ionic strength solutions were avoided.

β-HgS*(s)*$_{nano}$ Exposure Studies

To determine the stability of the particles under four environmental conditions (anoxic dark, anoxic light, oxic dark and oxic light), β-HgS*(s)*$_{nano}$ were prepared as described above using ELIS DOM as the capping agent. The solution was divided into four batches. Each reaction vial contained 3 mL of solution and this was purged with air (oxic) or nitrogen (anoxic) for 5 min at a rate of about 40 mL/min. Vials purged with N_2 were immediately capped and sealed with parafilm, and the vials under dark conditions were wrapped in foil. All vials were stored in the lab beside the window for the duration of the experiment. Though we report here that light exposure studies were conducted in sunlight, we acknowledge that both the vial (polypropylene centrifuge tube) and glass window attenuate the UV light reaching the sample, and so the role of UV in influencing β-HgS*(s)*$_{nano}$ was not directly assessed.

After three days of exposure, particle size of the β-HgS*(s)*$_{nano}$ was determined by DLS and compared to size obtained on day 1 upon synthesis of the particles. Following the DLS

measurements, vials were purged again with air/nitrogen as described above and those representing dark conditions were covered with foil. All vials were again left in the lab beside the window for 4 weeks during which time the vials were monitored for sedimentation. The experiment was later repeated under the same conditions except that blank vials containing DOM in 2.2 mM $NaHCO_3$ were added to the experiment. The blank vials represented each of the four conditions investigated with the β-HgS*(s)*$_{nano}$, and were conducted identical to and parallel with the repeat β-HgS*(s)*$_{nano}$ vials. Two sets of additional DOM blanks were left covered with foil inside the glovebox (lab blanks).

At the end of the exposure studies, an equal volume of 1 M $CaCl_2$ was added to all vials containing β-HgS*(s)*$_{nano}$ to cause particle sedimentation. 1 M $CaCl_2$ was also added to one set of the lab blanks to monitor the effect of $CaCl_2$ addition on the DOM. The rest of the DOM blanks were diluted with MQ to keep the dilution factors between the different sets of experiments equal. All vials containing $CaCl_2$ were centrifuged at 5000 rpm for 10 min and the supernatant collected and filtered through a 0.2 μm PTFE syringe filter. Specific Ultra Violet Absorption (SUVA) at 254 nm of the filtered solutions and of the rest of the blank solutions was then determined by multiplying the raw absorbance at 254 nm (A) with 2.303 and dividing with the path length in m (l) and the dissolved organic carbon (DOC) concentration in mg C/L (C) as shown in equation 1 below.

$$\mathrm{SUVA}_{254} = \frac{A_{254} \times 2.303}{l \times C} \qquad 1$$

Determining β-HgS*(s)*$_{nano}$ Particle Size

The β-HgS*(s)*$_{nano}$ particle size was determined by Dynamic Light Scattering (DLS) using a Malvern Zetasizer ZS90. After the appropriate reaction time, solutions containing β-HgS*(s)*$_{nano}$

were mixed then transferred to a 1 cm quartz cuvette and measurements taken at 25°C. The intensity-weighted hydrodynamic diameter was calculated from 20 individual measurements of 10 seconds each. The hydrodynamic diameter of β-HgS*(s)*$_{nano}$ was taken to be the size that corresponds to the peak with the highest intensity. For all samples except two, the major peak accounted for 70% of the scattering intensity. The two samples were β-HgS*(s)*$_{nano}$ solutions precipitated at a Hg^{II}:DOM ratio of 1.5 and 6.8 μmole Hg^{II} / mg C and whose major peak contributed 49 and 66 % of the scattering intensity, respectively. Since scattering intensity increases with the size of the particles, DLS measurements are biased towards larger particles and aggregates. Thus, the DLS diameter reported here does not necessarily correspond to the average size of the scattering particles, as it is not based on their population but rather is more reflective of how well aggregation and growth is hindered in one situation over another.

The scattering intensities of blank solutions containing Hg^{II}, DOM and $NaHCO_3$ were less than 1.5 kilocounts per sec (kcps) with the exception of when a high concentration of DOM was used (56 mM C), in which case it was 10.5 kcps. Scattering intensities of experimental solutions containing Hg^{II}, DOM and HS^- were above 5 kcps with most solutions above 10 kcps.

Samples were prepared for TEM by inserting the TEM grid in the β-HgS*(s)*$_{nano}$ solution and placing the solution on a shaker table for 30 minutes. The TEM grid was then removed and washed with 5μL of ultrapure water for more than 5 times. TEM images were captured using FEI –Talos high resolution microscope operated at an accelerating voltage of 200 KV as described in a previous study.[13]

Absorbance and Fluorescence Measurements

Absorbance measurements were conducted using a UV-Vis spectrophotometer (Hitachi U3010). Samples were analyzed in a 1 cm quartz cuvette using equimolar mixtures of 2.2 mM $NaHCO_3$ and MQ or 2.2mM $NaHCO_3$ and 1M $CaCl_2$ as the reference solution depending on the matrix of the sample to be measured. Fluorescence (FL) measurements were performed using a Hitachi F2000 fluorometer with a 1 cm quartz cuvette. Excitation Emission Matrices (EEMs) of DOM samples were performed on diluted samples (to minimize inner-filter effects) with an absorptivity of < 0.05 cm^{-1} at 220 nm.[42] FL scans of the DOM and matrix ($NaHCO_3$) were recorded using an excitation wavelength spanning from 220 to 450 nm, every 5 nm. The matrix EEM was subtracted from the sample EEM, after which the corrected sample EEMs were normalized to the intensity of the Raman peak of MQ water (at λ_{ex} of 350 nm and λ_{em} of 371–428 nm), recorded on each day of analysis.[43] The Raman and Rayleigh scattering peaks were removed from the sample EEMs by including only emission data for wavelengths 40 nm above the λ_{ex} and less than twice the excitation wavelength. For example, for λ_{ex} of 300 nm, emission data included in the EEM ranged from 341-600 nm.

Results

β-HgS*(s)*$_{nano}$ Formed using Different Capping Agents

The hydrodynamic diameter of β-HgS(s)$_{nano}$

The formation of β-HgS*(s)*$_{nano}$ was investigated using different thiols (cysteine, glutathione, 4-mercaptophenylacetic acid, 1,2-ethanedithiol, and 1,3-propanedithiol) and natural organic matter extracted from 3 marine environments (ELIS, WLIS and SB). We used a solid phase extraction technique with a Bond Elut PPL resin to extract dissolved organic matter.[36] The extraction efficiency for the DOM was 53%, and this is comparable to the extraction efficiency

reported for seawater using PPL cartridges.[36, 44] The formation of metacinnabar was not confirmed in these studies, however, the general procedure adopted for β-HgS*(s)*$_{nano}$ synthesis is similar to published procedures in studies where the formation of metacinnabar has been confirmed using X-ray Diffraction Crystallography, Energy Dispersive X-ray Spectroscopy and Extended X-ray Absorption Fine Structure.[27, 29, 31, 32]

Dynamic Light Scattering was used to monitor the hydrodynamic diameter of the β-HgS*(s)*$_{nano}$. Particles that formed in the presence of ELIS and WLIS DOM were comparable in size (about 12 nm) and were smaller than those formed in SB DOM, 28 nm (Fig. 1). Among the thiols, the smallest particles were formed in the presence of glutathione and 4-MAA (~ 6.5 nm) and these were about half the size of particles forming in the presence of cysteine (Fig. 2).

Particles that formed in the presence of the dithiols had a much larger (>100 nm) hydrodynamic diameter after 9h of reaction than those formed with the monothiols. These particles also settled within 10 days of reaction while those capped with the monothiols were stable in solution for over a month. Since DLS measures the hydrodynamic diameter, it does not provide the diameter of the core particle. Instead, the hydrodynamic diameter is determined from the diffusion coefficient of the sample and then assuming a spherical particle, the diameter is calculated using the Stokes- Einstein's equation. Since the diffusion coefficient of the particle is influenced by factors such as the water of hydration, the adsorbed ligand, and the aggregation state, the hydrodynamic diameter is also affected by these parameters and can be different from the actual size of the core particle.

The core particle diameter of β-HgS(s)$_{nano}$

We therefore also estimated the core diameter of the thiol capped β-HgS*(s)*$_{nano}$ from their UV-Vis spectra. This is possible because of the quantum confinement effect exhibited in

semiconductor NPs with sizes similar to their Bohr's radius.[45] The size of the particle is related to the energy difference between the band gap of the nanoparticle and that of the bulk material as described in the following equation:

$$\Delta E = E_{NP} - E_{bulk} = \frac{h^2}{8 R^2}\left(\frac{1}{m_e} + \frac{1}{m_h}\right) - \frac{1.8\, e^2}{4\, \varepsilon\, R \prod \varepsilon_o} \qquad (2)$$

where E is the band gap energy, m_e and m_h are the effective masses of the electron and hole respectively, e is the charge of an electron, ε_o is the permittivity of a vacuum, ε is the dielectric constant of the material, and R is the radius of the particle. To calculate the size of β-HgS*(s)*$_{nano}$, the following constants were used: E_{bulk} = 0.3 eV, ε = 11.4 m_e = 0.036 and m_h = 0.044.[46-48]

The band gap energy of a semiconductor is the energy required to excite an electron from the valence band to the conduction band. As the size of a semiconductor material decreases, the band gap energy increases, hence NPs have band gap energies larger than their bulk counterparts. The band gap energy of HgS*(s)*$_{nano}$ lies in the UV-Vis region and can be determined from absorbance measurements. The band gap energy of a nanoparticle is obtained by extending a line tangent to the absorption edge (where the peak sharply rises) to the x-axis.

The spectra of the β-HgS*(s)*$_{nano}$ are shown in Fig. 3 and the band gap energy of the β-HgS*(s)*$_{nano}$ capped with glutathione, cysteine, 1,2-ethanedithiol, and 1,3-propanedithiol were found to be 399, 403, 402, and 417 nm, respectively. As our samples were polydisperse, the peak did not rise as sharply and our calculations are estimates of the average particle size in the sample. Previous studies on CdS*(s)*$_{nano}$ have used fluorescence spectroscopy to verify that the absorbance of the NPs is due to an electronic transition rather than light scattering by the particles.[49] Here, fluorescence studies were not performed on the β-HgS*(s)*$_{nano}$, however, in preliminary experiments, cysteine capped β-HgS*(s)*$_{nano}$ and CdS*(s)*$_{nano}$ were prepared using

procedures similar to those outlined above with 150 μM HS^- and Hg^{II} /Cd^{II}, and 600 μM cysteine. While the emission of $CdS(s)_{nano}$ was clearly evident at around 550 nm when particles were excited at 350 nm, the emission spectra of β-$HgS(s)_{nano}$ was almost nonexistent when the particles were excited at 250 nm (Fig. S4). The sharp peaks in the fluorescence spectra of β-$HgS(s)_{nano}$ and $CdS(s)_{nano}$ correspond to Raman and second order Rayleigh scattering peaks. Low or missing fluorescence of β-$HgS(s)_{nano}$ has been reported in previous studies and is suggested to be due to the presence of intrinsic surface states with a higher probability of non-radiative decay process.[50, 51]

The practice of using absorbance measurements to calculate nanoparticle size is frequently employed in the literature to size engineered NPs. Its application to naturally forming nanomaterials is however debatable. Nanoparticles forming in natural settings tend to be poorly crystalline and contain more defects than engineered NPs. Estimating their particle size using constants belonging to their bulk and more crystalline counterparts could be uncertain. In spite of the mentioned concerns, we found during our preliminary experiments that the size of cysteine capped β-$HgS(s)_{nano}$ determined from absorbance measurements taken periodically over 23 days (5.4 ± 0.02 nm, Fig. S5) was reasonably similar to the size determined from TEM images of the particles (7.5 ± 1.5 nm, Fig. S6).

Most importantly, we would like to note that absorbance measurements were not used to determine the absolute size of β-$HgS(s)_{nano}$ formed in the presence of the different thiol ligands, but were rather used to examine if the large difference in particle size, as seen from the DLS measurements in Fig. 2, between β-$HgS(s)_{nano}$ formed in the presence of mono and dithiols was caused solely by a difference in core particle diameter. The core diameter of the dithiol capped particles was found not to be very different from the core diameter of particles formed in

presence of the monothiols (Table 1). This indicates that the much larger hydrodynamic diameter of the β-HgS*(s)*$_{nano}$ formed in the dithiols was mostly due to aggregation and not the growth of the core particle.

The growth of β-HgS(s)$_{nano}$ over time

The growth of β-HgS*(s)*$_{nano}$ was monitored for up to five weeks in experiments where the capping agent was ELIS DOM, SB DOM or cysteine. As in the previous experiment, β-HgS*(s)*$_{nano}$ were synthesized by adding 150 μM HS^- to a solution containing 150 μM Hg^{II} and 10 mg C/L (833 μM) DOM (ELIS/SB) or 150 μM Hg^{II} and 300 μM cysteine. The DLS measurement of the particles taken immediately after the addition of HS^- (5 min) gave an average particle size of 19.6 ± 3.6 nm for SB; 12.8 ± 1.7 nm for ELIS; and 9.9 ± 1.0 nm for cysteine. Particle size did not change significantly with time when monitored for up to 9 h (Fig. S7). At longer times (up to 5 weeks), particles capped with ELIS DOM did not show significant growth (Fig. 4a) while those capped with SB DOM doubled in size (Fig. 4b). In general, samples were quite polydisperse with a polydispersity index between 0.5 and 1.0 recorded by DLS for most samples. There was however, no trend related to the size distribution of particles between the two DOMs.

ELIS and SB DOM were characterized for their optical properties. The specific ultraviolet absorption (SUVA) for ELIS and SB DOM was determined by dividing the Napierian absorption coefficient at 254 nm with the concentration of the DOC in solution (equation 1) and found to be 4.9 and 2.5 L $mg^{-1}m^{-1}$ for ELIS and SB DOM, respectively. For comparison, Suwannee River Humic Acid (SRHA) has a SUVA value of 16.1 L $mg^{-1}m^{-1}$.[52] Furthermore, the 3D excitation and emission matrices of fluorescence scans (Fig. S8) show that ELIS has a higher fraction of humic-like materials (max emission at a longer wavelength) and a lower fraction of

proteinaceous-like materials (max emission at a shorter wavelength) than SB.[53-55] In addition, the total dissolved organic carbon to total nitrogen ratio (TDOC/TN) of the two DOMs were found to be 26.7 for SB DOM and 27.0 for ELIS DOM. We did not measure the concentration of sulfur for the DOM used here; however, the concentration of reduced sulfur groups for the DOM that was extracted in our lab from seawater collected from Long Island Sound south of Nantucket was found to be 0.058 mmol per g of organic matter. This value is about half of that determined by Manceau and Nagy for SRHA using XANES (0.11 mmol/g organic matter).[56] Similar to Manceau and Nagy, we used a Gaussian Curve fitting method to deconvolute the S XANES spectrum, however, while data for SRHA was fit to six standards, here XANES data was fit to eight standards to additionally include FeS and FeS_2. As the LIS DOM was extracted from surface waters, the concentration of mackinawite and pyrite in the DOM was not detected and thus still allows for its comparison with SRHA.

β-HgS*(s)*$_{nano}$ Formed at Different Hg^{II}:DOM Ratios

β-HgS*(s)*$_{nano}$ were formed in the presence of different amounts of ELIS DOM. Dissolved organic matter is composed of a mixture of organic molecules containing phenolic, carboxylic, amino, and thiol functional groups. As a soft acid, Hg^{II} forms stronger complexes with thiol containing moieties of the DOM than with moieties containing the other functional groups. The thiol functional groups on DOM are found however, at a much lower concentration than the O and N containing groups.[39] Thus, as the concentration of Hg^{II} increases relative to the DOM, the thiol groups become saturated and Hg^{II} then binds to weaker O and N containing groups.[39] The binding affinity of Hg^{II} to DOM therefore decreases with an increase in the Hg^{II}:DOM ratio. Using aquatic DOM, Haitzer *et al.,* showed that increasing the Hg^{II}:DOM ratio above 5 nmol

Hg^{II}/mg C decreased the binding affinity of Hg^{II} to DOM. Below 5 nmol Hg^{II}/mg C the binding affinity was high and constant.[40] Here, we varied the Hg^{II}:DOM ratio from 1.5 nmol Hg^{II}/mg C to 150 μmol Hg^{II} /mg C. As the Hg^{II}:DOM ratio increased (binding affinity reduced), particle size increased (Fig. 5). The β-HgS*(s)*$_{nano}$ in reaction vials containing a Hg^{II}:DOM ratio greater than 68 μmol Hg^{II} /mg C settled within a few minutes to one hour after the introduction of HS^-.

Between 6.8 and 41 μmol Hg^{II} /mg C, particle size increased gradually from an average of 6.5 ± 1.8 to 23.3 ± 1.0 nm, after which there was a sharp increase in particle size (Fig. 5a). At the two lowest ratios used (1.5 nmol and 1.5 μmol Hg^{II} /mg C) the particle diameter obtained from DLS measurements was 61.3 and 33 nm, respectively. TEM images of particles formed at 1.5 nmol Hg^{II} /mg C revealed that particles of ~5 nm in size were present amidst few large aggregates of up to 50 nm in size (Fig. S9). The lack of clarity in the TEM images was due to the low contrast between the particles and the background caused by the high concentration of organic matter that was present in the reaction vial (56 mM C).

TEM studies for particles precipitated at a ratio of 1.5 μmol Hg^{II} /mg C were not done here, however, an earlier study in our lab synthesized β-HgS*(s)*$_{nano}$ at a Hg^{II}:DOM ratio of 1 μmol Hg^{II}/ mg C using DOM extracted from Long Island Sound and following the procedure described here (except with a lower concentration of DOM). Particle diameter in this earlier study was determined using TEM and found to be 4.9 nm.[13]

The Stability of β-HgS*(s)*$_{nano}$ under Different Conditions

To contrast the results above which were completed under dark and anoxic conditions, the stability of β-HgS*(s)*$_{nano}$ was examined in sunlit and oxygenated conditions in the presence of ELIS DOM. The formed β-HgS*(s)*$_{nano}$ were purged with air or nitrogen before exposure to

light/dark conditions. Whereas the particles in dark conditions, whether purged with air or nitrogen, showed no or slight growth over time; exposure to sunlight led to a significant increase in particle size, from about 13 nm to 71 nm (Fig. 6). This experiment was subsequently repeated with enough blanks to monitor experimental artifacts. In the initial experiment, particles that were exposed to both air and light settled after two weeks, while the rest remained stable in solution for at least one month. In the repeat experiment, particles started settling in vials representing light oxic and light anoxic conditions after 12 h of exposure to sunlight.

Following particle sedimentation, the aromatic content of the DOM was analyzed by determining SUVA. NPs were first separated from solution by adding $CaCl_2$, centrifuging, and filtering through a 0.2 μm syringe filter, then absorbance and DOC measurements of the supernatant solutions were performed. In the initial experiment, we could not calculate SUVA accurately after the exposure studies as the DOC concentration in the supernatant solutions of all the vials measured was three time more than the anticipated concentration of 833 μM C. This was probably caused by a dilution that was not recorded in the notebook or was due to contamination from organic matter in the chemicals used to prepare the solutions. In the repeat experiment, the expected concentration was 854 μM, while the average DOC measured in all the vials at the end of the experiment was 970 ± 138 μM (14% more than the expected concentration).

During the repeat experiment, there was no difference in the SUVA of the DOM blank solutions exposed to the four conditions (anoxic dark, oxic dark, anoxic light and oxic light), and the values were comparable to the SUVA of the DOM blank that was stored covered in the glove box (lab blank) during the exposure studies (Table 2). In the experimental vials containing β-$HgS(s)_{nano}$, SUVA of the solutions in the light oxic and light anoxic conditions were slightly

lower than those of the solutions in the dark vials (Table 2). The light oxic vials however, had SUVA similar to the DOM blank that was left covered in the glove box during the exposure studies but had the whole process of $CaCl_2$ addition, centrifugation and filtration done alongside the vials containing β-HgS*(s)*$_{nano}$ ($CaCl_2$ lab blank). It is also important to note that although SUVA of the blank solutions were all higher than SUVA of the solutions in the β-HgS*(s)*$_{nano}$ vials, SUVA of the 'lab blank' was also higher than SUVA of the '$CaCl_2$ lab blank' (Table 2).

Discussion

Formation of β-HgS*(s)*$_{nano}$ with Different Capping Agents

All the thiols and organic matter used in this study stabilized β-HgS*(s)*$_{nano}$ well enough to prevent sedimentation during the course of the experiment. The stability can be assumed to be due to Hg^{II}-thiol binding and hydrophobic interactions between the surface of the particle and organic matter in solution, as has been suggested in previous studies.[23, 26, 29, 49] As there was no dramatic difference in the size of the core particles formed in the presence of the thiols (Fig. 3 and Table 1), the differences in the hydrodynamic diameter shown in Fig. 2 imply mainly differences in the ability of the organic compounds to hinder aggregation. Heavier capping agents and those with more aromatic content formed particles with a smaller hydrodynamic diameter than their counterparts (Figs.1 & S8), suggesting that at the Hg^{II}:DOM ratios used (15 μmol Hg^{II} / mg C), steric forces are important in the aggregation and growth of NPs. These results are consistent with the hypothesis that DOM with more humic character, such as coastal DOM, leads to NPs with a smaller diameter than those forming in the presence of oceanic DOM.

Our results are in line with previous studies, which found an inverse relation between molecular weight and aromaticity of the DOM with the size of β-HgS*(s)*$_{nano}$.[27, 29] Much larger

hydrodynamic diameters of the formed β-HgS*(s)*$_{nano}$ were obtained when propane and ethane dithiol were used as the capping agents (Fig. 2). Though this is consistent with their smaller molecular weight, it is also possible that the presence of two thiol groups on the capping agent caused inter-staple crosslinking between the NPs. Previous studies looking at Au, Pb and CdTe NPs have observed that multiple thiol groups in a capping agent bridge neighboring NPs.[57-59] Inter-staple cross-linking reduces the distance between two particles and is known to cause aggregation and sedimentation.[57] Here, while the particles capped with the monothiols remained suspended in solution, sedimentation occurred within 10 days of reaction when the dithiols were used. Thus, in addition to molecular weight and aromaticity, multiple thiol groups in a capping agent can affect the aggregation state of NPs forming in the environment.

Formation of β-HgS*(s)*$_{nano}$ at Different Hg^{II}:DOM Ratios

The relative concentration of DOM controls the aggregation of β-HgS(s)$_{nano}$

β-HgS*(s)*$_{nano}$ were formed under different ratios of Hg^{II}:DOM from 1.5 nmol – 150 μmol Hg^{II}/mg C. At intermediate ratios (6.8 – 41) of Hg^{II}:DOM used here, a linear relationship between the Hg^{II}:DOM ratio and the hydrodynamic size of the particles was observed (Fig. 5b). As mentioned earlier, the presence of a suitable organic molecule during particle formation hinders the growth/aggregation of particles. Growth typically occurs when new ions attach to a formed particle or when smaller particles collide, aggregate and then merge to form bigger and more stable particles.[22-24] Organic molecules adhere to the surface of a growing particle and rapidly undergo adsorption and desorption; a process that hinders the attachment of new ions and the collision and merger of two particles.[24, 60] When the relative concentration of organic matter is increased, more organic molecules compete for the adsorption sites on the β-HgS*(s)*$_{nano}$

surface; the desorption of one DOM molecule will be more rapidly followed by the adsorption of another molecule and the particle becomes well coated with DOM and more resistant to growth/aggregation. In our experiments, as the relative DOM concentration was decreased (Hg^{II}:DOM ratio increased), less organic molecules adsorbed on the particle surface decreasing the extent of DOM coating on the β-HgS*(s)*$_{nano}$. This likely led to the aggregation of particles with the extent of aggregation linearly dependent on the relative concentration of DOM (Fig. 5b). At a Hg^{II}:DOM ratio of 68 μmol Hg^{II} /mg C rapid aggregation occurred implying that the concentration of DOM was now too low to stabilize the particles. Although at the said ratio particles did not settle during the course of the experiment, sedimentation occurred within an hour of reaction for all other Hg^{II}:DOM ratios greater than 68 μmol Hg^{II} /mg C.

At the lowest two ratios of Hg^{II}:DOM used in this study (1.5 nmol and 1.5 μmol/ mg C), the hydrodynamic diameter of the formed β-HgS*(s)*$_{nano}$ were larger than the diameter of particles formed at higher ratios (Fig. 5a). This is contrary to expectation and to previous studies which have reported a decrease in the diameter of particles with increase in the concentration of DOM.[27] Although, the large hydrodynamic diameter of β-HgS*(s)*$_{nano}$ formed at 1.5 nmol Hg^{II} /mg C is supported by the presence of few large aggregates in the TEM images (Fig. S9), these aggregates could also have formed during the preparation of the TEM sample. As the β-HgS*(s)*$_{nano}$ were formed in an aqueous matrix, they are prone to aggregation when deposited on a carbon coated grid. In addition, since high concentrations of DOM were used to precipitate particles at 1.5 nmol and 1.5 μmol Hg^{II} / mg C (56 and 8.3 mM respectively), the higher than expected hydrodynamic diameter could have been due to the aggregation of DOM molecules at such high concentrations used. The DLS of a blank solution containing 56 mM DOM showed 2 peaks of about equal intensities which corresponded to particles of 5 mm and 36 nm in size. The

scattering intensity of the blank solution was, however, almost half that of the solution containing the same amount of DOM but with Hg^{II} and HS^- added (10.5 vs. 24.2 kcps). It is also possible that the large hydrodynamic diameters at the lower ratios may be due to an increase in the adsorbed DOM layer thickness. Large hydrodynamic diameters of Au and hematite particles have been detected under high DOM concentration or high ionic strength.[41, 61] It has been suggested that under these conditions, inter and intramolecular forces of DOM are screened resulting in an increased DOM adsorption.[41] To minimize repulsive forces between the adsorbed DOM molecules, the molecules adopt coiled structures that extend far into the solution.[41, 61] Adsorption layers up to 55 nm have been witnessed for hematite NPs stabilized with Aldrich humic acid.[61] An adsorption layer this large may however not be possible with our much lower molecular weight DOM. Future studies could use Time Resolved DLS measurements (to track changes in DLS diameter over time) coupled with Small Angle X-ray Scattering (SAXS) measurements of the β-$HgS(s)_{nano}$ at different Hg^{II}:DOM ratios to determine if particle aggregation is happening in solution or if an increase in DOM layer thickness is at all contributing to the large hydrodynamic diameter of β-$HgS(s)_{nano}$ precipitated at 1.5 nmol and 1.5 μmol Hg^{II} / mg C, as has been done in previous studies.[41]

Surface Hg atoms and functional groups on DOM

Using a core particle diameter of 5 nm, we calculated that 45% of Hg atoms will be on the surface of the nanoparticles. In our calculations, we used the volume of one HgS molecule (28.7 cm^3 mol^{-1}) and assumed that the particle surface is covered by a mono-layer of HgS monomers and that all the Hg atoms in this outermost layer are accessible from the surface. As the particles will have defects and vacancies which will affect the distribution of atoms within the crystal, our calculations are simply rough estimates of the fraction of surface atoms on the

formed β-HgS*(s)*$_{nano}$. These surface atoms are labile and may be more prone to dissolution. In terms of bioavailability of NPs, it has also been suggested that the labile surface atoms could interact with ligands present on the cell wall of Hg^{II} methylating bacteria and thereby facilitate their uptake and subsequent conversion of Hg^{II} to toxic MeHg.[12] Indeed β-HgS*(s)*$_{nano}$ have been found to be more bioavailable than β-HgS*(s)*$_{micro}$ to Hg^{II} methylating bacteria.[12, 13]

Our results showing an increase in β-HgS*(s)*$_{nano}$ particle size with decreasing concentration of organic matter are consistent with previous studies using fresh water and soil derived DOM.[27, 31] For example, it was found that in the presence of SRHA at a ratio of 3 μmol Hg^{II}/mg C, the NPs were ~ 50 nm, and increased with increasing Hg^{II}:DOM ratio to be >150 nm at a ratio of 12 μmol Hg^{II}/mg C.[27] Here we similarly show that high Hg^{II}:DOM ratios are required to induce aggregation and sedimentation. It is useful to consider the relative ratio of Hg^{II} to thiol ligands in the DOM under these conditions. Various investigators have estimated the number of thiol groups (RSH) in DOM and suggest that the mole ratio of RSH groups (exocyclic reduced sulfur groups) to DOC ranges from 0.0006 to 0.0009 mol RSH/mol C.[5, 39] As the concentration of thiols is suggested to comprise 30% of the pool of reduced organic sulfur, LIS DOM can be assumed to have a concentration of 0.0004 mol RSH/mol C while based on the results of Manceau and Nagy, SRHA will have a thiol concentration of 0.0008 mol RSH/mol C.[39, 56] Cleary, the thiol concentration for the DOM used here is lower than established in the previous studies using soil and stream organic matter. Using these ratios, we can estimate that above 41 μmol Hg^{II}/ mg C, where the particles started to aggregate rapidly, the mole ratio of surface Hg atoms to RSH groups was greater than 200; well above the maximum ratio of 1 expected to coordinatively saturate surface Hg^{II} atoms and offer sufficient stabilization against aggregation. This indicates that the stabilization of β-HgS*(s)*$_{nano}$ by DOM may not be entirely due

to covalent bonding between Hg atoms and thiol groups on DOM. Other ligands besides thiols, may be involved in the interaction with the nanoparticle surface. While previous studies have indicated that carboxylic acids are not effective in hindering the precipitation of β-HgS*(s)*$_{nano}$ even at low Hg^{II}:DOM ratios (0.8 μmol Hg^{II}/mg C), it is possible that amine groups and other strong binding sites within the DOM could also be involved in the stabilization of β-HgS*(s)*$_{nano}$.[27] Alternatively, bulky DOM molecules adsorbed on β-HgS*(s)*$_{nano}$ may have sterically blocked multiple binding sites on the particle surface rendering them inaccessible to thiol groups present on other DOM molecules. This phenomenon might explain why rapid aggregation of β-HgS*(s)*$_{nano}$ occurred at a much higher Hg^{II}:RSH mole ratio than expected. It is also possible that the β-HgS*(s)*$_{nano}$ stabilization effect is mainly through non-specific hydrophobic interactions between the organic capping agent and the surface of the particle.[26, 27] In such a case, the Hg^{II}:RSH mole ratio would say little about the stability of the β-HgS*(s)*$_{nano}$ solutions. We note that in calculating the mole ratio of surface Hg atoms to RSH, we assumed 100% yield of β-HgS*(s)*$_{nano}$. The actual yield is however much less than 100%, but since the unreacted Hg^{II} likely exists as bound to two thiol groups on DOM molecules, the ratio of Hg atoms on the surface of the particles to unbound thiol groups will be even higher than assumed above; further supporting the involvement of other functional groups or predominance of steric forces and hydrophobic interactions in the stabilization of the nanoparticles. Additional studies using model ligands with various functional groups and done at different Hg^{II}:DOM ratios could help to further determine the nature of nanoparticle stabilization by DOM.

Persistence of β-HgS*(s)*$_{nano}$ in the Environment

Short and long-term studies looking at the change in particle size for β-HgS*(s)*$_{nano}$ capped with cysteine and marine DOM, suggest that the diameter of the β-HgS*(s)*$_{nano}$ did not change appreciably with time (Fig. 4 & S7). This is similar to what previous studies have found for particles forming in Suwannee River humic and fulvic acid —a terrestrially derived DOM.[27, 32] Pham *et al.,* using Small Angle X-ray Scattering (SAXS) suggested that contrary to the DLS results, particles are in fact aggregating in solution.[32] It was argued that the constant diameter assessed by DLS was because the intensity weighted DLS measurements are biased towards bigger particles which were not increasing in size.[32] Other studies have shown that the Hg-S-DOM solution is in a state of dynamic equilibrium where the formation and dissolution of β-HgS*(s)*$_{nano}$ is happening continuously over time.[29] In our system, we monitored particles for over a month, and during this time the average growth rate was 0.6 and 4 nm/week for ELIS and SB DOM, respectively (Fig. 4). Also, no sedimentation was noticed during the entire period. Our results suggest that while it is possible that formation, aggregation, and dissolution of β-HgS*(s)*$_{nano}$ are all concurrently happening over time, the slight growth rate observed after 5 weeks indicates net aggregation may be a more dominant process, albeit happening at a slow rate.

Contrary to the slow growth of β-HgS*(s)*$_{nano}$ observed in dark anoxic conditions, rapid aggregation and growth happened when the solutions were purged with air and/or exposed to sunlight (Fig. 6). In addition, in the initial light exposure studies, sedimentation was noticed in the light oxic vials within two weeks of reaction while in the later experiments, sedimentation begun in the light oxic and light anoxic vials 12 h following light exposure. One could argue that sedimentation in the light vials occurred because of the photo-oxidation of aromatic components of organic matter. The SUVA measurements conducted at the end of the exposure studies

however, do not support the degradation of aromatic components of DOM. As shown in Table 2, SUVA of the DOM blank solutions were not altered during the exposure studies. Secondly, though at the end of the experiment, the solutions in the β-HgS*(s)*$_{nano}$ vials exposed to light had SUVA less than that of the starting DOM (4.9 L mg^{-1} m^{-1}), all solutions that had $CaCl_2$ added and had been centrifuged and filtered (including the $CaCl_2$ lab blank) showed a reduction in the SUVA value (Table 2). This suggests that the change in SUVA noted in the light β-HgS*(s)*$_{nano}$ vials, could not be due to the photodegradation of aromatic components of DOM and thus nullifies our third hypothesis. Instead, the change in SUVA could be a procedural artifact caused by the procedure adopted for separating β-HgS*(s)*$_{nano}$ from solution prior to the SUVA measurements. Previous studies have shown that the UV absorbance (and SUVA) of organic matter increased when filtrate turbidities were greater than 0.5 ntu.[62] The process of $CaCl_2$ addition, centrifugation and filtration therefore might have changed the turbidity status of the system and reduced the absorbance of DOM at 254 nm thus lowering the SUVA values of the solutions that had contained β-HgS*(s)*$_{nano}$.

Other than photo-oxidizing the DOM, presence of dissolved oxygen in the solutions might have caused the oxidative dissolution of β-HgS*(s)*$_{nano}$. Oxidative/reductive dissolution is known to occur for minerals containing elements that are redox-sensitive.[63] Both Hg and S undergo redox reactions, but only the oxidation of S^{2-} to SO_4^{2+} on HgS*(s)* has been shown to contribute to its dissolution.[63, 64] The rate of dissolution of cinnabar (α-HgS*(s)*) was found to be similar to the weathering of stable minerals like quartz.[65] Dissolution of cinnabar is enhanced in the presence of DOM and it has been suggested that aromatic components of DOM such as quinones could be involved in the oxidation.[66] The increase in the hydrodynamic diameter of β-HgS*(s)*$_{nano}$ upon exposure to light (Fig. 6) could thus be due to the dissolution of smaller sized β-

$HgS(s)_{nano}$ causing the particle size distribution to shift to larger particles. In our experiments, we cannot conclude whether or not dissolution occurred as the concentration of Hg^{II} and SO_4^{2-} in the solutions was not monitored over the course of the experiment. Future studies employing methods such as ultrafiltration would be able to monitor changes in the dissolved Hg^{II} concentration and elucidate to what extent dissolution is impacting the results. Nonetheless, since sedimentation occurred several days later in the vials exposed to light, our results suggest that aggregation rather than dissolution was the major process happening in the β-$HgS(s)_{nano}$ solutions exposed to light.

The rapid aggregation of β-$HgS(s)_{nano}$ following light exposure could have been caused by photochemical changes in the DOM resulting in DOM being less effective as a capping agent for β-$HgS(s)_{nano}$. For example, the production of reactive oxygen species upon irradiation could oxidize reduced organic sulfur groups on the DOM. As these are the functional groups that would preferentially bind to Hg atoms on the particle and prevent aggregation, their oxidation would compromise the effectiveness of DOM as a capping agent and may lead to particle aggregation. Overall, our results indicate that photo-induced changes in DOM affect the fate of β-$HgS(s)_{nano}$ forming in aquatic systems.

Conclusions and Environmental Implications

In this work, we used equimolar concentrations of mercury and sulfur to precipitate the NPs. The concentration of Hg^{II} used is unlikely to be found in the environment, where the concentration of mercury is substantially lower than that of sulfide, but higher concentrations of sulfide than used in our experiments are environmentally possible. Typical concentrations of mercury and sulfur in overlying waters and porewaters of pristine systems range from 10–600

pM and 0.1–1000 μM, respectively.[5, 7, 67] With speciation modeling using stability constants reported in our earlier study, a DOC concentration of 400 μM, pH of 7 and salinity of 20, the saturation index of β-HgS*(s)* (Q/K) was found to be greater than 1 for environments containing low nM concentrations of mercury and μM concentrations of sulfide (Fig. 7), similar to what has been reported in a previous study.[13, 27] This concentration of Hg^{II} and HS^- is close to what could be found in pristine systems, especially in environments such as sediment porewaters. Additionally, conditions conducive to precipitation and NP formation, would definitely occur in contaminated coastal environments, as previously suggested.[27] The presence of various other metal ions in solution could also cause Hg containing mixed metal sulfides to precipitate at much lower concentrations of mercury and sulfur than predicted above, as has been shown for iron phosphate particles.[21, 68] Also, we have preliminary evidence that Hg^{II} could associate, through cation exchange or other interactions, with other Group 12 NPs such as CdS*(s)*$_{nano}$, CdSe*(s)*$_{nano}$ and CdTe*(s)*$_{nano}$. As the binding of Hg^{II} to sulfide, selenide and telluride is much stronger than that of Cd^{II}, Hg^{II} could exchange with the cations in the matrix of these NPs, or be adsorbed on the particle surface.[69] Many manufactured NPs ("quantum dots") contain Cd^{II} bound to these Group 16 elements, and such exchange reactions could enhance the toxicity of quantum dots released into the environment. Further work is needed to examine such interactions more fully.

Here we have examined the stability of β-HgS*(s)*$_{nano}$ in low ionic strength media across a range of Hg^{II}:DOM ratios. Though we did not study the effect of ionic strength on the aggregation behavior of β-HgS*(s)*$_{nano}$, higher ionic strength solutions could exacerbate the aggregation rates and cause sedimentation even at low Hg^{II}:DOM ratios, as found in other studies.[70] An important avenue for future studies would be to determine the critical coagulation concentration (concentration of electrolyte needed to eliminate electrostatic repulsion between

particles) for β-HgS*(s)*$_{nano}$ formed at different Hg^{II}:DOM ratios and for the various capping agents used. The critical coagulation concentration is a good measure of colloidal stability and can be used to further compare the stabilizing effects of the different capping agents studied here.[41]

The presence of multivalent ions in solution is also likely to destabilize the NPs by bridging DOM molecules adsorbed on neighboring β-HgS*(s)*$_{nano}$, similar to the effect of the dithiols discussed earlier. Indeed, relatively small concentrations of Mg^{2+}, Ca^{2+}, and Al^{3+} induced the aggregation of CdTe quantum dots, yet they remained stable at high concentrations of KCl.[71] Even considering a well-coated particle, high concentrations of mono and divalent ions in solution can induce aggregation and sedimentation. The settled particles, however, can be expected to remain loosely bound due to the intercalation of the DOM molecules between the particles. Particles effectively coated by DOM but aggregating under high salt concentration could be re-suspended and disaggregated with mechanical perturbation.

Overall, we have shown that marine DOM stabilizes β-HgS*(s)*$_{nano}$ substantially in dark anoxic conditions and that the stabilization likely involves functional groups other than thiols. The use of marine DOM to precipitate β-HgS*(s)*$_{nano}$ has not been studied before. Additionally, as discussed in previous studies, there is evidence that Hg^{II} in the form of β-HgS*(s)*$_{nano}$ is more bioavailable to Hg^{II} methylating bacteria than micro-sized β-HgS*(s)*, although it is not as bioavailable as other Hg^{II} complexes.[13] Therefore, the presence of nanoparticles in marine sediments could affect the rate at which Hg^{II} is converted into MeHg. We also show for the first time that the transportation of β-HgS*(s)*$_{nano}$ from dark porewaters to surface waters, for example during sediment resuspension events, would impact the stability of the particles as DOM adsorbed on the surface of the particles could undergo photochemical transformation upon light

exposure rendering it less effective as a capping agent for β-HgS*(s)*$_{nano}$. Nanoparticles entering the marine surface waters can also be incorporated into marine snow and taken up by filter-feeders such as bivalves, as has been shown for TiO_2 nanoparticles.[72] The filtration size cutoff for filter-feeding organisms is typically a few microns and therefore these organisms would not assimilate NPs unless coagulation has occurred. The interactions outlined above could therefore substantially enhance the formation of Hg-containing NPs in environmental media and strongly impact their environmental fate and toxicity.

Acknowledgments

This work was supported by the National Science Foundation (NSF grant number 1607913). The TEM studies were performed in the UConn/FEI Center for Advanced Microscopy and Materials Analysis (CAMMA). S K-edge XANES were done on beamline 4B7A in Beijing Synchrotron Radiation Facilities in China. We thank Drs. Sofi Jonsson and Zofia Baumann for the useful comments during the preparation of the manuscript.

References

1. Compeau, G.C.; Bartha, R. Sulfate-reducing bacteria: Principal methylators of mercury in anoxic estuarine sediment. *Appl. Environ. Microbiol.* **1985,** *50* (2), 498-502.

2. Parks, J.M.; Johs, A.; Podar, M.; Bridou, R.; Hurt Jr., R.A.; Smith, S.D.; Tomanicek, S.J.; Qian, Y.; Brown, S.D.; Brandt, C.C.; Palumbo, A.V.; Smith, J.C.; Wall, J.D.; Elias, D.A.; Liang, L. The genetic basis for bacterial mercury methylation. *Science* **2013,** *339* (6125), 1332-1335; 10.1126/science.1230667.

3. Capone, D.G.; Kiene, R.P. Comparison of microbial dynamics in marine and freshwater sediments: Contrasts in anaerobic carbon catabolism. *Limnol. Oceanogr.* **1988,** *33* (4part2), 725-749; 10.4319/lo.1988.33.4part2.0725.

4. Mason, R.P.; Lawson, N.M.; Lawrence, A.L.; Leaner, J.J.; Lee, J.G.; Sheu, G.-. Mercury in the Chesapeake Bay. *Mar. Chem.* **1999,** *65* (1-2), 77-96.

5. Hollweg, T.A.; Gilmour, C.C.; Mason, R.P. Mercury and methylmercury cycling in sediments of the mid-Atlantic continental shelf and slope. *Limnol. Oceanogr.* **2010,** *55* (6), 2703-2722.

6. Benoit, J.M.; Gilmour, C.C.; Mason, R.P.; Heyes, A. Sulfide controls on mercury speciation and bioavailability to methylating bacteria in sediment pore waters. *Environ. Sci. Technol.* **1999,** *33* (6), 951-957; 10.1021/es9808200.

7. Schartup, A.T.; Mason, R.P.; Balcom, P.H.; Hollweg, T.A.; Chen, C.Y. Methylmercury production in estuarine sediments: Role of organic matter. *Environmental Science and Technology* **2013,** *47* (2), 695-700.

8. Schartup, A.T.; Balcom, P.H.; Mason, R.P. Sediment-porewater partitioning, total sulfur, and methylmercury production in estuaries. *Environ. Sci. Technol.* **2014,** *48* (2), 954-960; 10.1021/es403030d; 10.1021/es403030d.

9. Liu, B.; Schaider, L.A.; Mason, R.P.; Shine, J.P.; Rabalais, N.N.; Senn, D.B. Controls on methylmercury accumulation in northern Gulf of Mexico sediments. *Estuar. Coast. Shelf Sci.* **2015,** *159*, 50-59; 10.1016/j.ecss.2015.03.030.

10. Jonsson, S.; Skyllberg, U.; Nilsson, M.B.; Westlund, P.-.; Shchukarev, A.; Lundberg, E.; Björn, E. Mercury methylation rates for geochemically relevant HgII species in sediments. *Environmental Science and Technology* **2012,** *46* (21), 11653-11659.

11. Hsu-Kim, H.; Kucharzyk, K.H.; Zhang, T.; Deshusses, M.A. Mechanisms regulating mercury bioavailability for methylating microorganisms in the aquatic environment: A critical review. *Environ. Sci. Technol.* **2013,** *47* (6), 2441-2456; 10.1021/es304370g.

12. Zhang, T.; Kim, B.; Levard, C.; Reinsch, B.C.; Lowry, G.V.; Deshusses, M.A.; Hsu-Kim, H. Methylation of mercury by bacteria exposed to dissolved, nanoparticulate, and microparticulate mercuric sulfides. *Environmental Science and Technology* **2012,** *46* (13), 6950-6958.

13. Mazrui, N.M.; Jonsson, S.; Thota, S.; Zhao, J.; Mason, R.P. Enhanced availability of mercury bound to dissolved organic matter for methylation in marine sediments. *Geochim. Cosmochim. Acta* **2016,** *194*, 153-162; 10.1016/j.gca.2016.08.019.

14. Barnett, M.O.; Harris, L.A.; Turner, R.R.; Stevenson, R.J.; Henson, T.J.; Melton, R.C.; Hoffman, D.P. Formation of mercuric sulfide in soil. *Environ. Sci. Technol.* **1998,** *31* (11), 3037-3043; 10.1021/es960389j.

15. Labrenz, M.; Druschel, G.K.; Thomsen-Ebert, T.; Gilbert, B.; Welch, S.A.; Kemner, K.M.; Logan, G.A.; Summons, R.E.; De Stasio, G.; Bond, P.L.; Lai, B.; Kelly, S.D.; Banfield, J.F. Formation of sphalerite (ZnS) deposits in natural biofilms of sulfate-reducing bacteria. *Science* **2000,** *290* (5497), 1744-1747.

16. Hochella Jr., M.F.; Moore, J.N.; Putnis, C.V.; Putnis, A.; Kasama, T.; Eberl, D.D. Direct observation of heavy metal-mineral association from the Clark Fork River Superfund Complex: Implications for metal transport and bioavailability. *Geochim. Cosmochim. Acta* **2005,** *69* (7), 1651-1663.

17. Weber, F.-.; Voegelin, A.; Kaegi, R.; Kretzschmar, R. Contaminant mobilization by metallic copper and metal sulphide colloids in flooded soil. *Nature Geoscience* **2009,** *2* (4), 267-271.

18. Lowry, G.V.; Shaw, S.; Kim, C.S.; Rytuba, J.J.; Brown Jr., G.E. Macroscopic and microscopic observations of particle-facilitated mercury transport from New Idria and Sulphur Bank mercury mine tailings. *Environ. Sci. Technol.* **2004,** *38* (19), 5101-5111; 10.1021/es034636c.

19. Fitzsimmons, J.N.; John, S.G.; Marsay, C.M.; Hoffman, C.L.; Nicholas, S.L.; Toner, B.M.; German, C.R.; Sherrell, R.M. Iron persistence in a distal hydrothermal plume supported by dissolved-particulate exchange. *Nature Geoscience* **2017,** *10*, 195-201.

20. Fitzsimmons, J.N.; Carrasco, G.G.; Wu, J.; Roshan, S.; Hatta, M.; Measures, C.I.; Conway, T.M.; John, S.G.; Boyle, E.A. Partitioning of dissolved iron and iron isotopes into soluble and colloidal phases along the GA03 GEOTRACES North Atlantic Transect. *Deep-Sea Research II* **2015,** *116*, 130-151.

21. Hochella, M.F.,Jr; Lower, S.K.; Maurice, P.A.; Penn, R.L.; Sahai, N.; Sparks, D.L.; Twining, B.S. Nanominerals, mineral nanoparticles, and Earth systems. *Science* **2008,** *319* (5870), 1631-1635; 10.1126/science.1141134; 10.1126/science.1141134.

22. Polte, J. Fundamental growth principles of colloidal metal nanoparticles - a new perspective. *Crystengcomm* **2015,** *17* (36), 6809-6830; 10.1039/c5ce01014d.

23. Mullaugh, K.M.; Luther III, G.W. Growth kinetics and long-term stability of CdS nanoparticles in aqueous solution under ambient conditions. *Journal of Nanoparticle Research* **2011,** *13* (1), 393-404.

24. Yin, Y.; Alivisatos, A.P. Colloidal nanocrystal synthesis and the organic-inorganic interface. *Nature* **2005,** *437* (7059), 664-670; 10.1038/nature04165.

25. Boles, M.A.; Ling, D.; Hyeon, T.; Talapin, D.V. The surface science of nanocrystals. *Nat. Mater.* **2016,** *15* (2), 141-153; 10.1038/nmat4526.

26. Ravichandran, M.; Aiken, G.R.; Ryan, J.N.; Reddy, M.M. Inhibition of precipitation and aggregation of metacinnabar (mercuric sulfide) by dissolved organic matter isolated from the Florida Everglades. *Environ. Sci. Technol.* **1999,** *33* (9), 1418-1423; 10.1021/es9811187.

27. Deonarine, A.; Hsu-Kim, H. Precipitation of mercuric sulfide nanoparticles in NOM-containing water: Implications for the natural environment. *Environmental Science and Technology* **2009,** *43* (7), 2368-2373.

28. Lau, B.L.T.; Hsu-Kim, H. Precipitation and growth of zinc sulfide nanoparticles in the presence of thiol-containing natural organic ligands. *Environ. Sci. Technol.* **2008,** *42* (19), 7236-7241; 10.1021/es801360b.

29. Slowey, A.J. Rate of formation and dissolution of mercury sulfide nanoparticles: The dual role of natural organic matter. *Geochim. Cosmochim. Acta* **2010,** *74* (16), 4693-4708.

30. Philippe, A.; Schaumann, G.E. Interactions of dissolved organic matter with natural and engineered inorganic colloids: A review. *Environ. Sci. Technol.* **2014,** *48* (16), 8946-8962; 10.1021/es502342r.

31. Gerbig, C.A.; Kim, C.S.; Stegemeier, J.P.; Ryan, J.N.; Aiken, G.R. Formation of nanocolloidal metacinnabar in mercury-DOM-sulfide systems. *Environ. Sci. Technol.* **2011,** *45* (21), 9180-9187; 10.1021/es201837h.

32. Pham, A.L.T.; Morris, A.; Zhang, T.; Ticknor, J.; Levard, C.; Hsu-Kim, H. Precipitation of nanoscale mercuric sulfides in the presence of natural organic matter: Structural properties, aggregation, and biotransformation. *Geochim. Cosmochim. Acta* **2014,** *133*, 204-215; 10.1016/j.gca.2014.02.027.

33. Kalnejais, L.H.; Martin, W.R.; Signell, R.P.; Bothner, M.H. Role of sediment resuspension in the remobilization of particulate-phase metals from coastal sediments. *Environ. Sci. Technol.* **2007,** *41* (7), 2282-2288; 10.1021/es061770z.

34. Hu, H.; Mylon, S.E.; Benoit, G. Distribution of the thiols glutathione and 3-mercaptopropionic acid in Connecticut lakes. *Limnol. Oceanogr.* **2006,** *51* (6), 2763-2774.

35. Ndu, U.C. The Mechanisms and Pathways of the Uptake of Inorganic Mercury and Methylmercury Species in Escherichia coli: Possible Implications for Mercury Cycling in the Marine Environment . Doctoral, University of Connecticut, DigitalCommons@Uconn, 2011.

36. Dittmar, T.; Koch, B.; Hertkorn, N.; Kattner, G. A simple and efficient method for the solid-phase extraction of dissolved organic matter (SPE-DOM) from seawater. *Limnol. Oceanogr. Methods* **2008,** *6* (JUN), 230-235.

37. Brouwer, H.; Murphy, T.P. Diffusion method for the determination of acid-volatile sulfides (AVS) in sediment. *Environ. Toxicol. Chem.* **1994,** *13* (8), 1273-1275.

38. Miller, C.L.; Southworth, G.; Brooks, S.; Liang, L.; Gu, B. Kinetic controls on the complexation between mercury and dissolved organic matter in a contaminated environment. *Environ. Sci. Technol.* **2009,** *43* (22), 8548-8553; 10.1021/es901891t.

39. Skyllberg, U.; Bloom, P.R.; Qian, J.; Lin, C.-.; Bleam, W.F. Complexation of mercury(II) in soil organic matter: EXAFS evidence for linear two-coordination with reduced sulfur groups. *Environmental Science and Technology* **2006,** *40* (13), 4174-4180.

40. Haitzer, M.; Aiken, G.R.; Ryan, J.N. Binding of mercury(II) to dissolved organic matter: The role of the mercury-to-DOM concentration ratio. *Environ. Sci. Technol.* **2002,** *36* (16), 3564-3570; 10.1021/es025699i.

41. Nason, J.A.; McDowell, S.A.; Callahan, T.W. Effects of natural organic matter type and concentration on the aggregation of citrate-stabilized gold nanoparticles. *Journal of Environmental Monitoring* **2012,** *14* (7), 1885-1892.

42. Burdige, D.J.; Kline, S.W.; Chen, W. Fluorescent dissolved organic matter in marine sediment pore waters. *Mar. Chem.* **2004,** *89* (1-4), 289-311; 10.1016/j.marchem.2004.02.015.

43. Lawaetz, A.J.; Stedmon, C.A. Fluorescence intensity calibration using the Raman scatter peak of water. *Appl. Spectrosc.* **2009,** *63* (8), 936-940; 10.1366/000370209788964548.

44. Green, N.W.; Perdue, E.M.; Aiken, G.R.; Butler, K.D.; Chen, H.; Dittmar, T.; Niggemann, J.; Stubbins, A. An intercomparison of three methods for the large-scale isolation of oceanic dissolved organic matter. *Mar. Chem.* **2014,** *161*, 14-19; 10.1016/j.marchem.2014.01.012.

45. Wang, Y.; Herron, N. Nanometer-sized semiconductor clusters: Materials synthesis, quantum size effects, and photophysical properties. *J. Phys. Chem.* **1991,** *95* (2), 525-532.

46. Mews, A.; Eychmueller, A.; Giersig, M.; Schooss, D.; Weller, H. Preparation, characterization, and photophysics of the quantum dot quantum well system CdS/HgS/CdS. *J. Phys. Chem.* **1994,** *98* (3), 934-941.

47. Long, Y.; Jiang, D.; Zhu, X.; Wang, J.; Zhou, F. Trace Hg 2+ analysis via quenching of the fluorescence of a CdS-encapsulated DNA nanocomposite. *Anal. Chem.* **2009,** *81* (7), 2652-2657; 10.1021/ac802592r.

48. Planelles, J.; Royo, M.; Pi, M. Nonparabolicity and dielectric effects on addition energy spectra of spherical nanocrystals. *J. Appl. Phys.* **2007,** *102* (9); 10.1063/1.2803722.

49. Mullaugh, K.M.; Luther III, G.W. Spectroscopic determination of the size of cadmium sulfide nanoparticles formed under environmentally relevant conditions. *Journal of Environmental Monitoring* **2010,** *12* (4), 890-897.

50. Mehta, S.K.; Kumar, S.; Chaudhary, S.; Bhasin, K.K. Nucleation and growth of surfactant-passivated CdS and HgS nanoparticles: Time-dependent absorption and luminescence profiles. *Nanoscale* **2010,** *2* (1), 145-152; 10.1039/b9nr00070d; 10.1039/b9nr00070d.

51. Yang, J.; Hu, Y.; Luo, J.; Zhu, Y.-.; Yu, J.-. Highly fluorescent, near-infrared-emitting Cd2+-Tuned HgS nanocrystals with optical applications. *Langmuir* **2015,** *31* (11), 3500-3509; 10.1021/la504879m.

52. Wenk, J.; Aeschbacher, M.; Salhi, E.; Canonica, S.; von Gunten, U.; Sander, M. Chemical oxidation of dissolved organic matter by chlorine dioxide, chlorine, and ozone: effects on its optical and antioxidant properties. *Environ. Sci. Technol.* **2013,** *47* (19), 11147-11156; 10.1021/es402516b [doi].

53. Para, J.; Coble, P.G.; Charrière, B.; Tedetti, M.; Fontana, C.; Sempéré, R. Fluorescence and absorption properties of chromophoric dissolved organic matter (CDOM) in coastal surface waters of the northwestern Mediterranean Sea, influence of the Rhône River. *Biogeosciences* **2010,** *7* (12), 4083-4103; 10.5194/bg-7-4083-2010.

54. Yamashita, Y.; Tanoue, E. Chemical characterization of protein-like fluorophores in DOM in relation to aromatic amino acids. *Mar. Chem.* **2003,** *82* (3-4), 255-271.

55. Coble, P.G.; Green, S.A.; Blough, N.V.; Gagosian, R.B. Characterization of dissolved organic matter in the Black Sea by fluorescence spectroscopy. *Nature* **1990,** *348* (6300), 432-435.

56. Manceau, A.; Nagy, K.L. Quantitative analysis of sulfur functional groups in natural organic matter by XANES spectroscopy. *Geochim. Cosmochim. Acta* **2012,** *99*, 206-223; 10.1016/j.gca.2012.09.033.

57. McPhail, M.R.; Campbell, G.P.; Bedzyk, M.J.; Weiss, E.A. Structural Features of PbS Nanocube Monolayers upon Treatment with Mono- and Dicarboxylic Acids and Thiols at a Liquid-Air Interface. *Langmuir* **2016,** *32* (26), 6666-6673; 10.1021/acs.langmuir.6b01444.

58. Jupally, V.R.; Kota, R.; Dornshuld, E.V.; Mattern, D.L.; Tschumper, G.S.; Jiang, D.-.; Dass, A. Interstaple dithiol cross-linking in Au 25(SR) 18 nanomolecules: A combined mass spectrometric and computational study. *J. Am. Chem. Soc.* **2011,** *133* (50), 20258-20266; 10.1021/ja206436x.

59. Koole, R.; Luigjes, B.; Tachiya, M.; Pool, R.; Vlugt, T.J.H.; De Mello Donegá, C.; Meijerink, A.; Vanmaekelbergh, D. Differences in cross-link chemistry between rigid and flexible dithiol molecules revealed by optical studies of CdTe quantum dots. *J. Phys. Chem. C* **2007,** *111* (30), 11208-11215; 10.1021/jp072407x.

60. Peng, X.; Manna, L.; Yang, W.; Wickham, J.; Scher, E.; Kadavanich, A.; Alivisatos, A.P. Shape control of CdSe nanocrystals. *Nature* **2000,** *404* (6773), 59-61; 10.1038/35003535.

61. Vermeer, A.W.P.; Van Riemsdijk, W.H.; Koopal, L.K. Adsorption of humic acid to mineral particles. 1. Specific and electrostatic interactions. *Langmuir* **1998,** *14* (10), 2810-2815.

62. Karanfil, T.; Erdogan, I.; Schlautman, M. The impact of filtrate turbidity on UV 254 and SUVA 254 determinations. *J. Am. Water Works Assoc.* **2005,** *97* (5), 125-136.

63. Ravichandran, M.; Aiken, G.R.; Reddy, M.M.; Ryan, J.N. Enhanced dissolution of cinnabar (mercuric sulfide) by dissolved organic matter isolated from the Florida Everglades. *Environ. Sci. Technol.* **1998,** *32* (21), 3305-3311; 10.1021/es9804058.

64. Holley, E.A.; James McQuillan, A.; Craw, D.; Kim, J.P.; Sander, S.G. Mercury mobilization by oxidative dissolution of cinnabar (a-HgS) and metacinnabar (ß-HgS). *Chem. Geol.* **2007,** *240* (3-4), 313-325; 10.1016/j.chemgeo.2007.03.001.

65. Barnett, M.O.; Turner, R.R.; Singer, P.C. Oxidative dissolution of metacinnabar (ß-HgS) by dissolved oxygen. *Appl. Geochem.* **2001,** *16* (13), 1499-1512; 10.1016/S0883-2927(01)00026-9.

66. Waples, J.S.; Nagy, K.L.; Aiken, G.R.; Ryan, J.N. Dissolution of cinnabar (HgS) in the presence of natural organic matter. *Geochim. Cosmochim. Acta* **2005,** *69* (6), 1575-1588; 10.1016/j.gca.2004.09.029.

67. Balcom, P.H.; Schartup, A.T.; Mason, R.P.; Chen, C.Y. Sources of water column methylmercury across multiple estuaries in the Northeast U.S. *Mar. Chem.* **2015,** *177*, 721-730; 10.1016/j.marchem.2015.10.012.

68. Sahai, N.; Lee, Y.J.; Xu, H.; Ciardelli, M.; Gaillard, J.-. Role of Fe(II) and phosphate in arsenic uptake by coprecipitation. *Geochim. Cosmochim. Acta* **2007,** *71* (13), 3193-3210; 10.1016/j.gca.2007.04.008.

69. Mazrui, N.M. The Interaction of Mercury and Methylmercury with Reduced Sulfur: Implications for the Transformation of Mercury and Methylmercury in the Environment. Ph.D, University of Connecticut, Storrs, CT, 2016.

70. Doyle, J.J.; Palumbo, V.; Huey, B.D.; Ward, J.E. Behavior of titanium dioxide nanoparticles in three aqueous media samples: Agglomeration and implications for benthic deposition. *Water Air Soil Pollut.* **2014,** *225* (9); 10.1007/s11270-014-2106-7.

71. Zhang, Y.; Chen, Y.; Westerhoff, P.; Crittenden, J.C. Stability and removal of water soluble CdTe quantum dots in water. *Environ. Sci. Technol.* **2008,** *42* (1), 321-325; 10.1021/es0714991.

72. Doyle, J.J.; Ward, J.E.; Mason, R. An examination of the ingestion, bioaccumulation, and depuration of titanium dioxide nanoparticles by the blue mussel (Mytilus edulis) and the eastern oyster (Crassostrea virginica). *Mar. Environ. Res.* **2015,** *110*, 45-52; 10.1016/j.marenvres.2015.07.020.

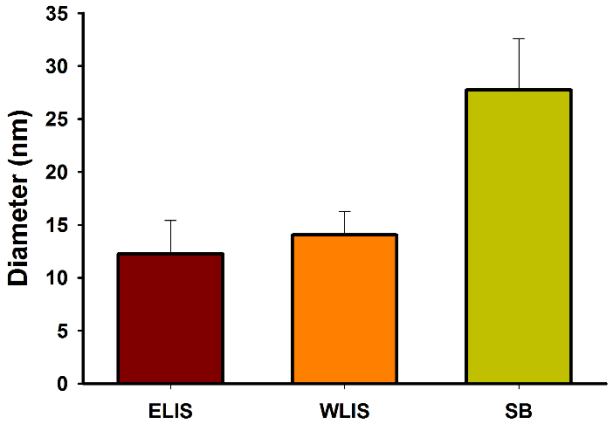

Fig. 1. The hydrodynamic diameter (mean ± SD, n=3) of DOM capped β-HgS*(s)*$_{nano}$. Solutions contained 150 µM $Hg(NO_3)_2$, 150 µM Na_2S and 10 mg C/L DOM extracted from Eastern Long Island Sound (ELIS), Western Long Island Sound (WLIS) and at the SB of the North Atlantic Ocean (SB), in 2.2 mM $NaHCO_3$ (pH 7.8). Measurements were taken 9h after reaction was initiated.

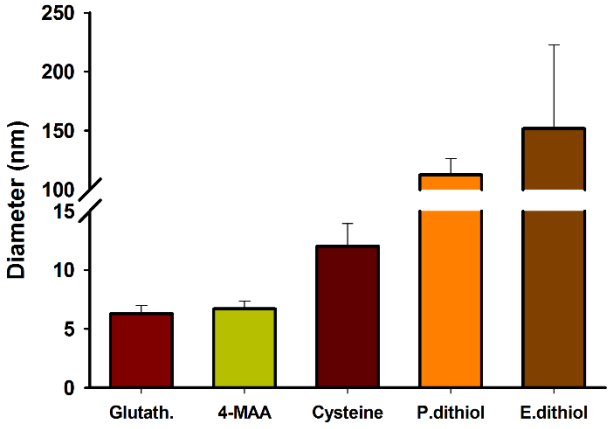

Fig. 2. The hydrodynamic diameter (mean ± SD, n=3) of thiol capped β-HgS*(s)*$_{nano}$. Solutions contained 150 µM $Hg(NO_3)_2$, 150 µM Na_2S and 300 µM monothiol (glutathione, mercaptophenyl acetic acid (4-MAA) or cysteine), or 150 µM dithiol (1,3-propanedithiol or 1,2-ethanedithiol), in 2.2 mM $NaHCO_3$ (pH 7.8). Measurements were taken 9h after reaction was initiated.

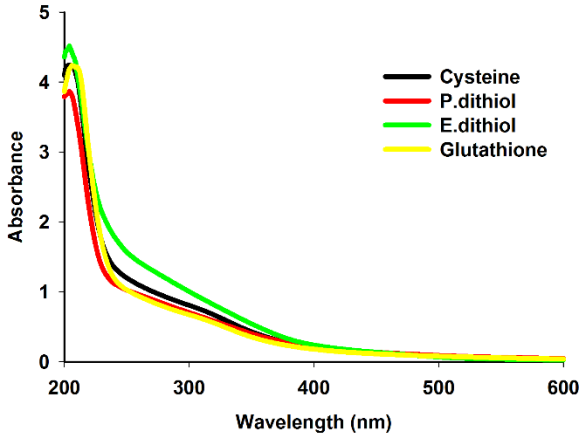

Fig. 3. The UV-Vis spectra of thiol capped β-HgS*(s)*$_{nano}$. The solutions contained 150 µM $Hg(NO_3)_2$, 150 µM Na_2S and 300 µM monothiol (cysteine or glutathione) or 150 µM dithiol (1,3-propanedithiol or 1,2-ethanedithiol), in 2.2 mM $NaHCO_3$ (pH 7.8). Measurements were taken 9h after reaction was initiated.

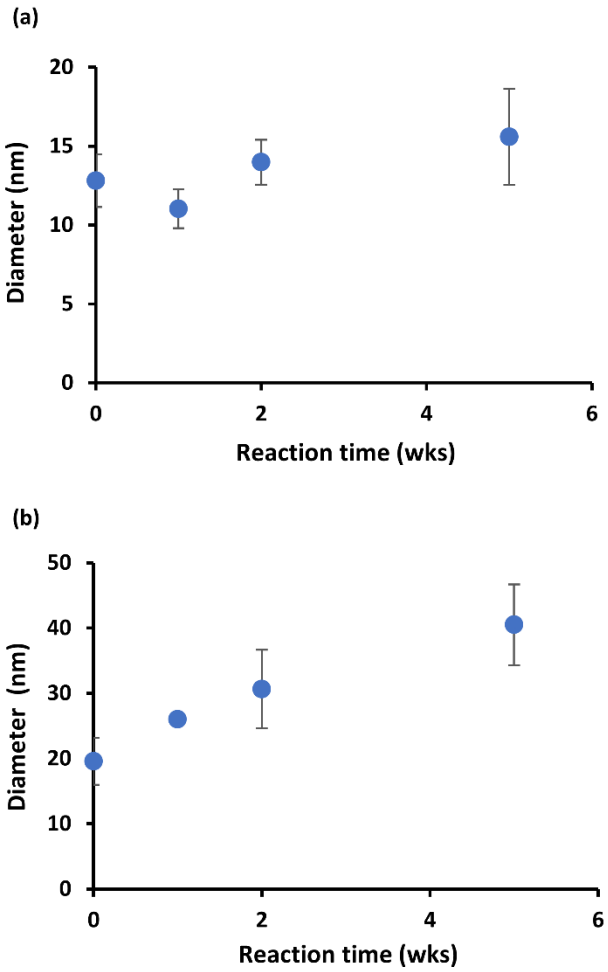

Fig. 4. The hydrodynamic diameter (mean ± SD, n=3) of β-HgS$(s)_{nano}$ monitored over time for up to 5 weeks. Solutions contained 150 µM $Hg(NO_3)_2$, 150 µM Na_2S and 10 mg C/L ELIS DOM (a) and SB DOM (b) in 2.2 mM $NaHCO_3$ (pH 7.8).

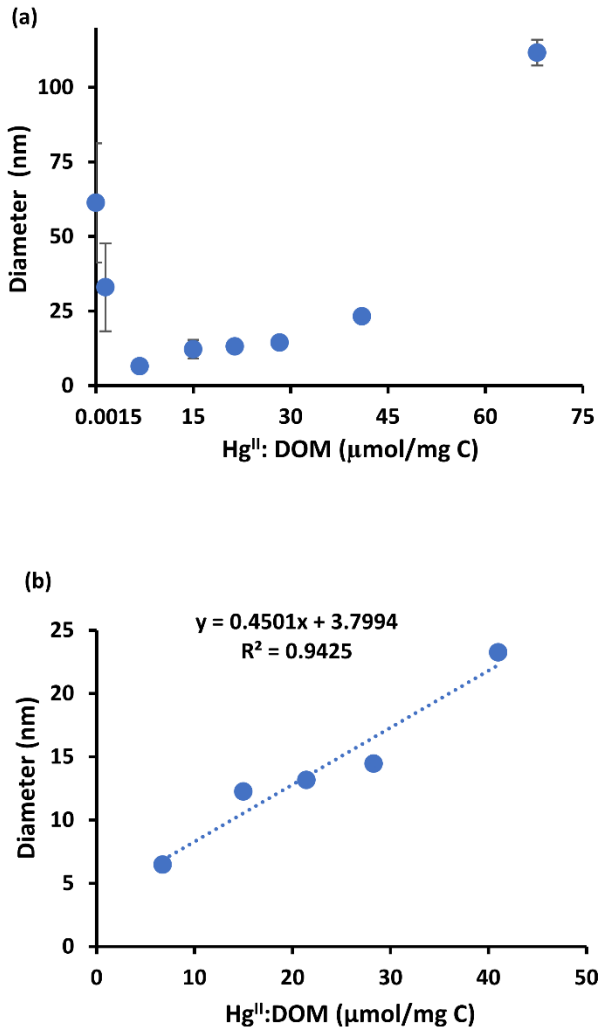

Fig. 5. The hydrodynamic diameter (mean ± SD, n=3) of β-HgS*(s)*$_{nano}$ precipitated at different ratios of Hg^{II}:DOM from 1.5 nmol – 68 µmol/mg C (a); and linear relation between the diameter of the β-HgS*(s)*$_{nano}$ and the Hg^{II}:DOM ratio obtained from 6.8–41 µmol/mg C (b). Solutions contained 150 µM $Hg(NO_3)_2$, 150 µM Na_2S and ELIS DOM in 2.2 mM $NaHCO_3$ (pH 7.8). Measurements were taken 9h after reaction was initiated.

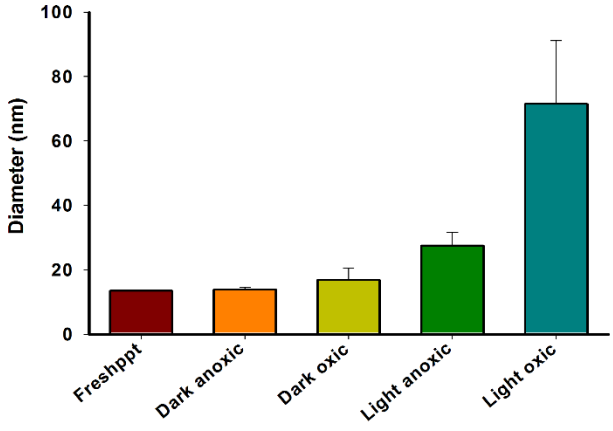

Fig. 6. The hydrodynamic diameter (mean ± SD, n=3) of β-HgS*(s)*$_{nano}$ freshly precipitated (1 day) and when the fresh precipitate was exposed to different environmental conditions (dark + nitrogen, dark + air, light + nitrogen and light + air) for 3 days. Solutions contained 150 µM $Hg(NO_3)_2$, 150 µM Na_2S and 10 mg C/L ELIS DOM in 2.2 mM $NaHCO_3$ (pH 7.8).

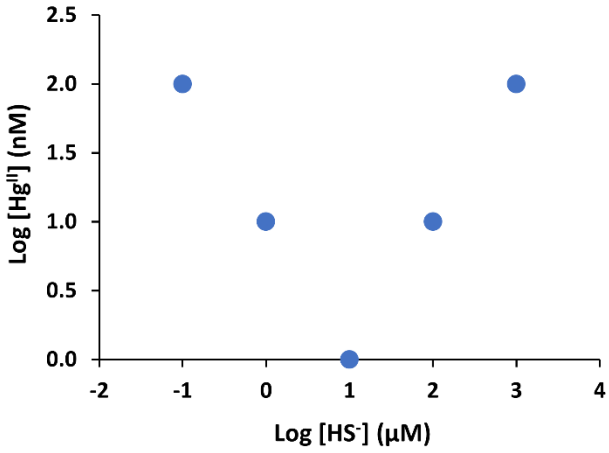

Fig. 7. Minimum theoretical concentration of Hg^{II} required to cause the precipitation of β-HgS*(s)* at a given concentration of HS^-.

Table 1: The core particle diameters of β-HgS*(s)*$_{nano}$ capped with glutathione, cysteine, 1,2-ethanedithiol, and 1,3-propanedithiol determined from the Effective Mass Approximation theory.

Ligand	UV-Vis Diameter (nm)
Glutathione	5.38
Cysteine	5.41
1,2-ethanedithiol	5.40
1,3-propanedithiol	5.51

Table 2: Specific Ultra Violet Absorption (SUVA) of filtrates of experimental solutions which contained DOM blank or β-HgS*(s)*$_{nano}$ after exposure to oxic/anoxic and light/dark conditions.

Experiment	SUVA
Lab blk	4.9 ± 0.3
Dark anoxic blk	4.9 ± 1.3
Dark oxic blk	4.9 ± 0.9
Light anoxic blk	4.9 ± 0.1
Light oxic blk	4.6 ± 0.1
Lab CaCl2 blk	3.3 ± 0.1
Dark anoxic NPs	3.8 ± 0.2
Dark oxic NPs	4.2 ± 0.2
Light anoxic NPs	2.8 ± 0.3
Light oxic NPs	3.3 ± 0.4